

# An X-ray view of the very faint black hole X-ray transient Swift J1357.2–0933 during its 2011 outburst

M. Armas Padilla<sup>1\*</sup>, R. Wijnands<sup>1</sup>, D. Altamirano<sup>1</sup>, M. Méndez<sup>2</sup>, J. M. Miller<sup>3</sup> and N. Degenaar<sup>3†</sup>

<sup>1</sup>*Astronomical Institute “Anton Pannekoek”, University of Amsterdam, Postbus 94249, 1090 GE Amsterdam, The Netherlands*

<sup>2</sup>*Kapteyn Astronomical Institute, University of Groningen, Postbus 800, 9700 AV Groningen, The Netherlands*

<sup>3</sup>*Department of Astronomy, University of Michigan, 500 Church Street, Ann Arbor, MI 48109, USA*

DRAFT VERSION

## ABSTRACT

We report on the X-ray spectral (using *XMM-Newton* data) and timing behavior (using *XMM-Newton* and *Rossi X-ray Timing Explorer [RXTE]* data) of the very faint X-ray transient and black hole system Swift J1357.2–0933 during its 2011 outburst. The *XMM-Newton* X-ray spectrum of this source can be adequately fitted with a soft thermal component with a temperature of  $\sim 0.22$  keV (using a disc model) and a hard, non-thermal component with a photon index of  $\Gamma \sim 1.6$  when using a simple power-law model. In addition, an edge at  $\sim 0.73$  keV is needed likely due to interstellar absorption. During the first *RXTE* observation we find a 6 mHz quasi-periodic oscillation (QPO) which is not present during any of the later *RXTE* observations or during the *XMM-Newton* observation which was taken 3 days after the first *RXTE* observation. The nature of this QPO is not clear but it could be related to a similar QPO seen in the black hole system H 1743–322 and to the so-called 1 Hz QPO seen in the dipping neutron-star X-ray binaries (although this latter identification is quite speculative). The observed QPO has similar frequencies as the optical dips seen previously in this source during its 2011 outburst but we cannot conclusively determine that they are due to the same underlying physical mechanism. Besides the QPO, we detect strong band-limited noise in the power-density spectra of the source (as calculated from both the *RXTE* and the *XMM-Newton* data) with characteristic frequencies and strengths very similar to other black hole X-ray transients when they are at low X-ray luminosities. We discuss the spectral and timing properties of the source in the context of the proposed very high inclination of this source. We conclude that all the phenomena seen from the source cannot, as yet, be straightforwardly explained neither by an edge-on configuration nor by any other inclination configuration of the orbit.

**Key words:** accretion, accretion discs - stars: individuals (Swift J1357.2–0933) - stars: black hole - X-rays: binaries

## 1 INTRODUCTION

In our Galaxy, the brightest X-ray emission originating from point sources is produced by binary systems harbouring a black hole or neutron star that is accreting material from a (sub)solar mass companion star. However, the X-ray luminosity exhibited by these low mass X-ray binaries (LMXBs) can vary by several orders of magnitude, in particular in the so-called X-ray transients. Those sources are a subgroup of LMXBs that spend most of their time in a quiescent state

with a low X-ray luminosity ( $L_X \sim 10^{30} - 10^{33}$  erg s<sup>-1</sup>), and sporadically transit to an outburst episode, in which the accretion rate increases drastically, resulting in several orders of magnitude increase in their X-ray brightness. These systems can be classified based on their 2–10 keV peak luminosity ( $L_X^{peak}$ ) reached during outbursts. Very faint X-ray transients (VFXTs; Wijnands et al. 2006) are those systems that reach  $L_X^{peak}$  of only  $\sim 10^{34} - 10^{36}$  erg s<sup>-1</sup>, orders of magnitude lower than the brighter, regular systems (which display  $L_X^{peak} \sim 10^{36} - 10^{39}$  erg s<sup>-1</sup>).

The low X-ray luminosities in combination with the duration of their outburst and quiescent episodes (i.e., duty cycles) imply that the VFXTs accrete at very low rates, both

\* e-mail: m.armaspadilla@uva.nl

† Hubble Fellow

instantaneously as well as averaged over many outbursts-quiescence cycles (Degenaar & Wijnands 2009, 2010). In fact, some of these sub-luminous sources might have such long-term time-averaged inferred mass-accretion rates that exotic evolution scenarios are necessary to explain their existence (King & Wijnands 2006; Wijnands et al. 2006; Degenaar & Wijnands 2009). A large fraction of the VFXTs has conclusively been identified as accreting neutron star systems by the detection of thermonuclear X-ray bursts (e.g., Maeda et al. 1996; Cornelisse et al. 2002; Chelovekov & Grebenev 2007; Del Santo et al. 2007; Wijnands et al. 2009; Degenaar & Wijnands 2010) but for the majority of VFXTs, the nature of the accretor remains elusive.

Swift J1357.2-0933 is so far the only confirmed black hole VFXT (Armas Padilla et al. 2013; Corral-Santana et al. 2013). The source was discovered in outburst on January 28, 2011 with the Swift Burst Alert Telescope (BAT; Barthelmy et al. 2005; Krimm et al. 2011a). Subsequent observations were carried out with several X-ray satellites as well as ground-based telescopes (e.g., Krimm et al. 2011b; Milisavljevic et al. 2011; Torres et al. 2011; Casares et al. 2011). The X-ray outburst lasted  $\sim 7$  months (e.g., see Fig. 1, top panel) and reached a 2–10 keV X-ray peak luminosity of  $L_X^{peak} \sim 10^{35}$  erg s $^{-1}$  which classified the system as VFXT (Armas Padilla et al. 2013). Photometry of the possible counterpart found in archival Sloan Digital Sky Survey (SDSS) data (at times when the source is assumed not to be active) indicated that the quiescent optical counterpart is very red and that the companion is likely an M4 star. From this, the distance toward the source was estimated to be  $\sim 1.5$  kpc (Rau et al. 2011; Corral-Santana et al. 2013).

Its short distance and the low Galactic extinction toward the source (due to its location above the Galactic plane;  $b=50.0042$ ), made it possible to obtain good UV/optical observations during outburst in addition to the X-ray observations. From optical data obtained during outburst, Corral-Santana et al. (2013) established the black hole nature for the accretor (they obtained a minimum mass of the accretor of  $M_x > 3.6 M_\odot$ ) and they found a 2.8 hours orbital period. In the same work they presented the detection of intense dips in the optical light curve, which were explained by a toroidal structure in the inner region of the disc seen at high inclination ( $i \gtrsim 70^\circ$ ) which is moving outward as the outburst progresses.

Optical and infrared observations obtained in 2012 and 2013 when the source was in quiescence (Shahbaz et al. 2013), revealed similar dips as seen during outburst as well as flare events. The light-curves were dominated by a larger variability than what is observed in other systems at similar time-resolution, which suggests that another source of light with large variability completely dominates the optical flux of the companion star (the companion star could not be detected). Shahbaz et al. (2013) estimated that the magnitude of the companion star is  $V_{min} = 22 - 25$ , which, combined with the expected magnitude for a M4.5 V secondary star, resulted in a inferred distance between 0.5 kpc and 6.3 kpc.

Using the X-ray and UV/optical data obtained with *Swift* during the 2011 outburst of Swift J1357.2-0933, Armas Padilla et al. (2013) found that the X-ray spectrum of the source softened with decreasing source luminosity and

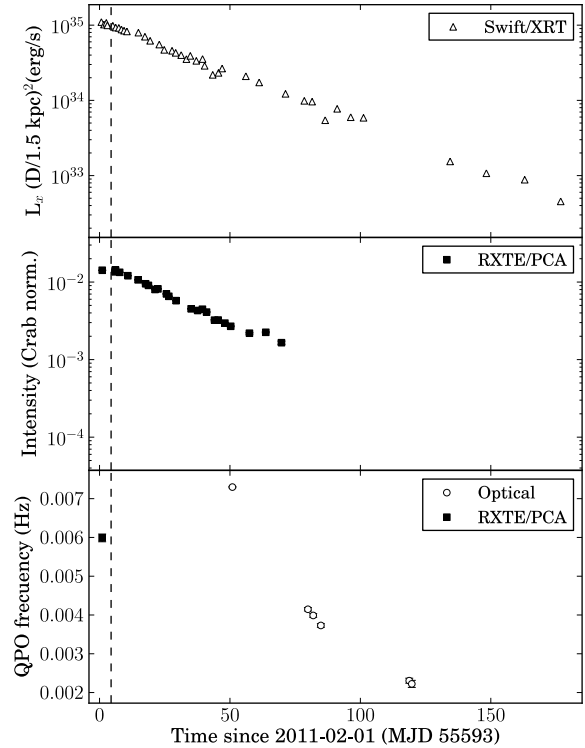


**Figure 1.** The *Swift*/XTE light-curve (top panel; from Armas Padilla et al. 2013) and the *RXTE*/PCA light-curve (middle panel) of the outburst of Swift J1357.2-0933. Bottom panel: The evolution of the frequency of the mHz QPOs seen in *RXTE* data (black square) and in the optical (white circles; from Corral-Santana et al. 2013). The dashed-line indicates when the *XMM-Newton* observation was performed.

that the X-ray flux was correlated with the UV and optical magnitudes in such a way that it is likely that the black hole is accreting via a non irradiated or only marginally irradiated disc.

In this paper, we present the spectral analysis of our *XMM-Newton* observation of Swift J1357.2-0933 obtained a few days after the peak of the X-ray outburst. We also present a timing study using the same *XMM-Newton* data in combination with data obtained throughout the outburst using the *Rossi X-ray Timing Explorer* (*RXTE*).

## 2 OBSERVATIONS AND ANALYSIS

### 2.1 *RXTE* observations

We used data from the *RXTE* Proportional Counter Array (PCA; for instrument information see Zhang et al. 1993). There were 26 pointed observations (all ObsID starting with 96065-02 and 96419-01), each consisting of a fraction of one to three entire satellite orbits. We used the 16-s time-resolution Standard 2 mode data to calculate the 2–20 keV intensity as described in Altamirano et al. (2008). We sub-

tracted the background and corrected for the deadtime. In order to correct for differences in effective area between the PCUs themselves, we normalized our intensity by the corresponding Crab color values (see Altamirano et al. 2008, for more details about this method). We used all active PCUs to calculate the average intensity per observation. The results are plotted in Fig. 1 (middle panel).

For the Fourier timing analysis we used the data obtained using the Good Xenon mode, which has a time resolution of  $\sim 1\mu\text{s}$ . Leahy-normalized power density spectra (PDS) were constructed using data segments of both 128 and 512 s. No background or deadtime corrections were made prior to the calculation of the power spectra. We first averaged the power spectra per observation. We inspected the shape of the average power spectra at high frequency ( $> 2000$  Hz) for unusual features in addition to the usual Poisson noise but none were found. We then subtracted the Poisson noise by estimating it from the power between 3000 and 4000 Hz, where neither intrinsic noise nor QPOs are known to be present, using the method developed by Klein Wolt (2004) based on the analytical function of Zhang et al. (1995). The resulting power spectra were converted to squared fractional rms (Belloni & Hasinger 1990; Miyamoto et al. 1991; van der Klis 1995). In this normalization the square root of the integrated power density equals the variance of the intrinsic variability in the source count rate.

## 2.2 XMM-Newton observation

The *XMM-Newton* observatory (Jansen et al. 2001) pointed at Swift J1357.2–0933 for  $\sim 37$  ks on 2011 February 5 (Obs ID 0674580101). In the current paper, we are using the data obtained with the European Photon Imaging Camera (EPIC) which contains two MOS cameras (Turner et al. 2001) and one PN camera (Strüder et al. 2001), as well as the data from the Reflection Grating Spectrometers (RGS, den Herder et al. 2001). During the observation the medium optical blocking filter was used. The MOS1 camera was operated in the small window imaging mode, while the MOS2 and PN cameras were operated in timing mode. To reduce the data we used the Science Analysis Software (SAS, v. 12.0).

In order to omit episodes of background flaring we excluded the data where the high-energy count rate was larger than  $0.25$  counts  $\text{s}^{-1}$  ( $>10$  keV) and  $0.6$  counts  $\text{s}^{-1}$  (10–12 keV) for the MOS and PN cameras, respectively, which resulted in a total live time of  $\sim 29$  ks. We used the task EPATPLOT to assess the presence of pile-up in our data. MOS1 was strongly affected (the source count rate is  $\sim 25$  counts  $\text{s}^{-1}$  when the pile-up starts to be an issue at count rates  $> 5$  counts  $\text{s}^{-1}$ ). In order to avoid the pile-up it is necessary to eliminate a large central portion (annular extraction region with a  $13''$  inner radius and a  $40''$  outer radius) which results in a very low statistic spectrum. Therefore we decide to exclude the MOS1 data from our analysis. We also excluded the MOS2 data because of the large uncertainties which still exist in the calibration of timing data obtained using this instrument.

We extracted the PN source and background events using the RAWX columns in [30:45] and in [2:9], respectively. The net source count rate is  $\sim 150$  counts  $\text{s}^{-1}$  (0.4–11 keV),

which is much lower than the  $\sim 800$  counts  $\text{s}^{-1}$  at which the pile-up starts to affect the observation. However, the EPATPLOT tool suggests that the observation is affected by pile-up and it is necessary to exclude the three central columns (RAWX columns in [37:39]) to mitigate the effects. We generated the spectrum for both column selections and compared them, and found that the two spectra are fully consistent with each other. Therefore, we concluded our observation was not affected or at most only slightly affected by pile-up and do not exclude any central columns from our source selection. We have also compared the spectrum when the background is subtracted and when it is not subtracted. When the PN CCD is operated in timing mode, bright sources might illuminate the entire CCD so that background spectra will be contaminated by photons from the source (e.g., Dunn et al. 2010; Hiemstra et al. 2011). However, there is no spectral shape difference between the background-subtracted spectrum and the one without background subtraction. For completeness, we still have corrected for the background in our analysis. We generated the light curves and the spectra, as well as the associated response matrix files (RMFs) and ancillary response files (ARFs) using the standard analysis threads<sup>1</sup>.

We used the SAS task RGSPROC to reduce the RGS data and to produce the response matrices and spectra. We selected the option keepcool=no and withrectification=yes. The first option excludes columns that give signals a few percent below the values expected from their immediately neighbours and are only likely to be relevant when studying weak absorption features in spectra with high statistics (see SAS User guide section 5.6.3; Díaz Trigo et al. 2012). The second option activates the current calibration file (CCF) that causes the empirical rectification correction factors, to be applied to RGS effective area to bring simultaneous models of RGS and EPIC-PN spectra into agreement by reducing apparent systematic errors to the level of better than about 1% (see the XMM-Newton CCF release note XMM-CCF-REL-269).

### 2.2.1 Spectral analysis

All spectra were grouped to contain a minimum of 25 photons per bin and the energy resolution was not oversampled by more than a factor 3. We fitted all spectra using XSPEC (v. 12.8; Arnaud 1996). We included the photoelectric absorption component (PHABS) to account for the interstellar absorption assuming the cross-sections of Verner et al. (1996) and the abundances of Wilms et al. (2000).

We combined the 0.4–1.8 keV RGS spectra (RGS1 and RGS2 first order) and the 0.7–10 keV EPIC-PN spectrum and fitted them simultaneously with the parameters tied between the three detectors. We added a constant factor (CONSTANT) to the spectral models with a value fixed to 1 for EPIC-PN spectrum and free to vary for the RGS spectra in order to account for cross calibrations uncertainties. We added a 1% systematic errors to all instruments to account for the errors in the relative calibration between the RGS and EPIC-PN detectors (Kirsch et al. 2004, XMM-SOC-CAL-TN-0052).

<sup>1</sup> <http://xmm.esac.esa.int/sas/current/documentation/threads/>

**Table 1.** Best fit to the 0.4–1.8 keV RGSs spectra and 0.7–10 keV PN spectrum using PHABS\*(DISKBB+NTHCOMP)\*EDGE.

Parameter [unit]		
	PHABS	
$N_{\text{H}} [\times 10^{12} \text{cm}^{-2}]$		3.52
	DISKBB	
$kT_{\text{in}} [\text{keV}]$		$0.216 \pm 0.005$
$N_{\text{Diskbb}}$		$1176 \pm 70$
	NTHCOMP	
$\Gamma$		$1.61 \pm 0.01$
$kT_{\text{e}} [\text{keV}]$		$8.23^{+1.57}_{-1.04}$
$kT_{\text{bb}} [\text{keV}]$		0.216 (tied)
$N_{\text{comp}}$		$0.0420 \pm 0.0003$
	EDGE	
edgeE [keV]		$0.731 \pm 0.005$
MaxTau		$0.10 \pm 0.01$
$F_{\text{X,abs}} [\times 10^{-10} \text{erg cm}^{-2} \text{s}^{-1}]$		$3.34 \pm 0.04$
$F_{\text{X,unabs}} [\times 10^{-10} \text{erg cm}^{-2} \text{s}^{-1}]$		$3.34 \pm 0.04$
$L_{\text{X}} [\times 10^{34} \text{erg s}^{-1}]$		$8.99 \pm 0.04$
Thermal fraction		6.6%
$\chi^2(\text{dof})$		1.08 (1136)

<sup>Note</sup> To calculate the parameter errors, we fixed the instrumental features components.

### 2.2.2 Timing analysis

Leahy-normalized power spectra were constructed (in segments of  $\sim 537$  s; no background or deadtime corrections were applied during this) using the *XMM-Newton*/PN data in the 0.5–10 keV energy range and using the same source extraction region as we used during the spectral analysis. We added all power spectra together to get an averaged one for the whole observation. We subtracted the Poisson noise spectrum, which was estimated for frequencies between 100 and 200 Hz. The power spectrum was converted to squared fractional rms in the same way as the *RXTE* data (see Section 2.1).

## 3 RESULTS

### 3.1 Spectral results

The first model which we used to fit the *XMM-Newton* spectrum was a power-law (POWERLAW) model with an accretion disc model consisting of multiple blackbody components (DISKBB; Makishima et al. 1986). With a  $\chi^2_{\nu}$  of 1.3 for 1146 degrees of freedom (dof) the fit was not acceptable (with a p-value<sup>2</sup> of  $\sim 1.9 \times 10^{-9}$ ). The residuals (Fig. 2(a)) showed an emission feature at  $\sim 2.2$  keV, likely produced by an over-compensation by the CTI correction in the characteristic EPIC-PN residual due to the Gold (2.21 keV) edge (Kolehmainen et al. 2013, in prep.). We added a Gaussian component (GAUSS) in our models to mitigate this instrumental feature. Additionally, the RGS spectra show residuals at  $\sim 0.54$  keV and  $\sim 0.65$  keV energies, possibly due to instrumental inefficiencies at the oxygen and iron edges, respectively (see the RGS calibration status XMM-SOC-CAL-TN-0030), and which were not accurately corrected in the

<sup>2</sup> The p-value represents the probability that the deviations between the data and the model are due to chance alone. In general, a model can be rejected when the p-value is smaller than 0.05.

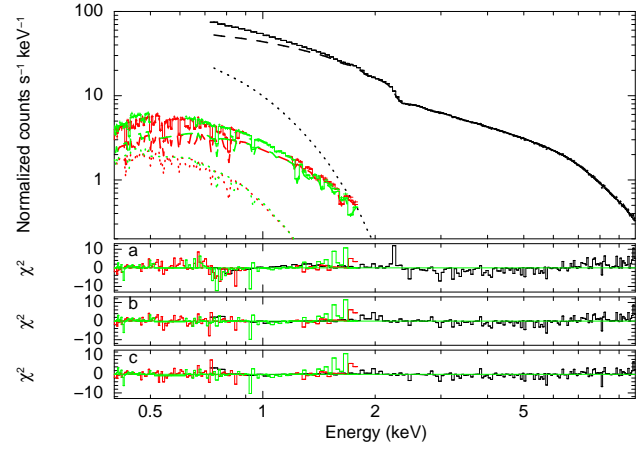


**Figure 2.** PN (black), RGS1 (red) and RGS2 (green) spectra. The solid lines represent the best fit for a combined NTHCOMP (dashes), DISKBB (dotted lines) and EDGE (at  $\sim 0.73$  keV) model. In the sub-panels the contributions to  $\chi^2$  are plotted when fitting with a) PHABS\*(DISKBB+PO) (without instrumental features corrections), b) PHABS\*(DISKBB+PO)\*EDGE and c) PHABS\*(DISKBB+NTHCOMP)\*EDGE.

calibration process. Therefore, we included two components (EDGE) in our fits to model such features. From now on, unless otherwise mentioned, we include these instrumental feature components in all our models.

The residuals also show an absorption feature at  $\sim 0.73$  keV. The interpretation for this feature can be absorption by interstellar iron L2 ( $\sim 0.73$  keV) or L3 ( $\sim 0.71$  keV) (Wilms et al. 2000; Díaz Trigo et al. 2007; Pinto et al. 2013). We incorporated an EDGE component to reproduce this feature in our models.

Once we had added these additional components to model the residuals (Fig. 2(b)), the fit with the DISKBB+POWERLAW model improves considerably ( $\chi^2_{\nu} \sim 1.13$  for 1137 dof) although still it is not an acceptable fit (with a p-value of  $\sim 0.002$ ). The disc temperature obtained was  $\sim 0.25$  keV and the photon index of the power-law component was  $\Gamma \sim 1.51$ . The photon index is in agreement with the values reported by Armas Padilla et al. (2013) in their analysis of the quasi-simultaneous *Swift* data of the source ( $\sim 1$  day of difference between the *XMM-Newton* and *Swift* observations). The unabsorbed 0.5–10 keV flux is  $3.3 \times 10^{-10} \text{erg cm}^{-2} \text{s}^{-1}$ , to which the thermal component contributes  $\sim 7\%$ . Assuming a distance of 1.5 kpc the inferred X-ray luminosity is  $L_{\text{X}} \sim 8.9 \times 10^{34} \text{erg s}^{-1}$ .

We repeated the fit replacing the hard POWERLAW component with a thermally comptonized continuum model (NTHCOMP; Zdziarski et al. 1996; Życki et al. 1999). We tied the seed photon temperature (low energy rollover;  $kT_{\text{bb}}$ ) to the diskbb temperature ( $T_{\text{in}}$ ). This change in the model to fit the hard component slightly reduces the  $\chi^2_{\nu}$  to 1.08 for 1136 dof (with a p-value of  $\sim 0.03$ ). The power-law photon index is  $\Gamma \sim 1.6$ , the diskbb temperature  $\sim 0.22$  keV and the electron temperature (high energy rollover;  $kT_{\text{e}}$ ) is  $\sim 8$  keV. The flux obtained using this model is the same than with the power-law component. We also repeated the fits replacing the DISKBB with the DISKPN (Gierliński et al. 1999), which is an extension of the DISKBB model that includes correc-



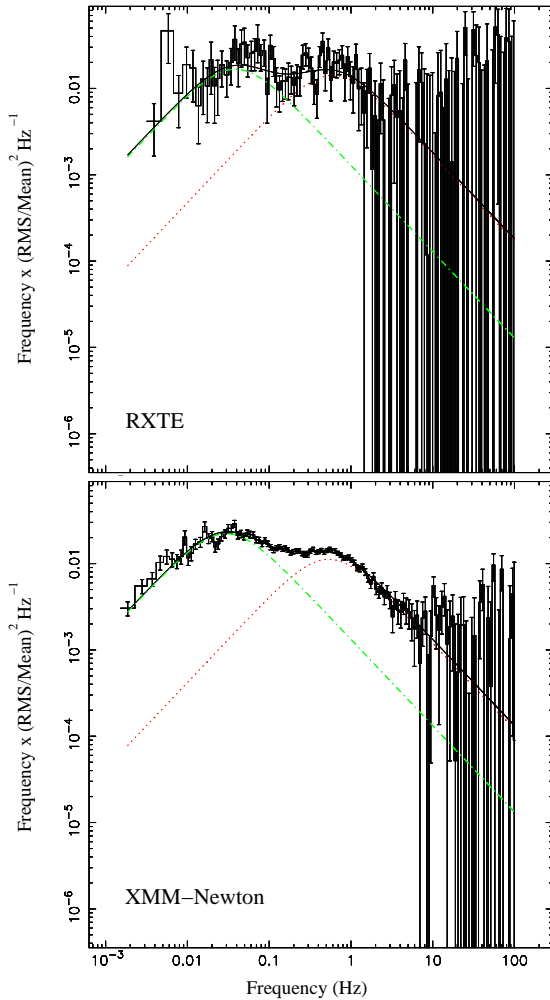


**Figure 3.** *Top panel:* Broad-band PDS (2–20 keV) of the first *RXTE* observation (ObsID: 96065-02-01-00; 2 Feb 2011). Clearly a strong broad-band noise is present, but below 0.01 Hz also the mHz QPO is visible. *Bottom panel:* Broad-band PDS (0.5–10 keV) of the *XMM-Newton*/PN observation performed on 5 Feb 2011. This also clearly shows the strong broad-band noise, but no evidence for the mHz QPO. In both panels, the dotted and dashed-dotted lines are the best fit model assuming two Lorentzians.

tions for temperature distribution near the black hole. However, the results were nearly identical when using the DISKBB model.

The impossibility to decrease the  $\chi^2_\nu$  and get an acceptable fit could be due to remaining uncertainties in the cross-calibration between the different detectors (e.g. we can see in Fig. 2 that there is a big contribution to the  $\chi^2$  in the overlapping between the EPIC-PN and RGS2 cameras between 1–2 keV). The results of the best spectral analysis (PHABS\*(DISKBB+NTHCOMP)\*EDGE) are reported in Table 1. The uncertainties on the spectral parameters are at 90% confidence level and the flux errors have been calculated following the procedure presented by Wijnands et al. (2004).

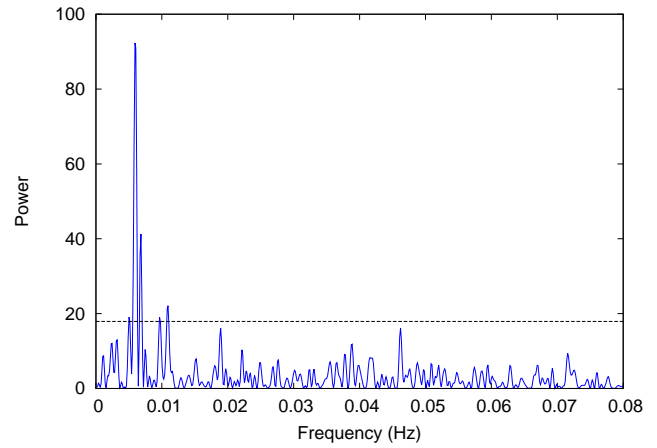


**Figure 4.** The Lomb-Scargle diagram of the *RXTE* observation performed on 2 Feb 2011 (ObsID: 96065-02-01-00) clearly showing the mHz QPO. The dashed line is the  $4\sigma$  significance level (assuming no red noise contribution).

### 3.2 Timing results

The power spectrum of the first *RXTE* observation (ObsID 96065-02-01-00;  $\sim 2$  ks obtained on 2 Feb 2011) is shown in Fig. 3 (top panel). Clearly a strong broad-band noise component is present which has a total rms amplitude (between 0.01 and 100 Hz) of  $35\pm 4\%$  (2–20 keV). We fitted the PDS using two zero-centered Lorentzians (Belloni et al. 2002). The obtained characteristic frequencies and fractional rms amplitudes (2–20 keV) of the two components are  $0.6\pm 0.1$  Hz and  $0.039\pm 0.007$  Hz, and  $21\pm 1\%$  and  $23\pm 1\%$ , respectively. The power spectra obtained for the other *RXTE* observations look very similar to this power spectrum, but with decreasing quality because of the decreasing count rate as the outburst progressed.

From Fig. 3, top panel, it can be seen that in the PDS of the first *RXTE* observation excess power is present at a frequency of  $\sim 0.005$  Hz. The PDS shows indications of a peak at  $\sim 6$  mHz. To investigate this feature further we used 1-s resolution GoodXenon mode PCA light curves in the  $\approx 2 - 60$  keV range and searched for periodicities in each *RXTE* orbit separately using Lomb-Scargle periodograms (Lomb 1976; Scargle 1982). The Lomb-Scargle periodogram of the first *RXTE* observation (which was one orbit long) is shown in Fig. 4, showing clearly a quasi-periodic oscillation (QPO) at  $5.9\pm 0.1$  mHz, with a FWHM  $< 2$  mHz (and thus quality factor of  $\sim 3$  or larger). The rms amplitude (2–60 keV) of this QPO is  $12\pm 3\%$ . We also searched the other *RXTE* observations for a similar frequency QPO, but none were found. However, given the low count rate and the length of the observations the upper limits are not constraining (the 3 sigma upper limits are typically of the order of tens of percent fractional rms). Since the second *RXTE* observation (ObsID: 96065-02-02-00) was performed on 7 Feb 2011, this means that the QPO lasted less than 5 days after the first *RXTE* observation.

The power spectrum of our *XMM-Newton* data is shown in Fig. 3 (bottom panel). Clearly a similar broad-band noise (with a total 0.5–10 keV rms amplitude between 0.01 and 100 Hz of  $33\pm 2\%$ ) is seen as in the *RXTE* data (Fig. 3, top panel), but without the mHz QPO. The 3 sigma upper

limit on the strength of a possible QPO is 7% rms in the 0.5–10 keV energy range. Since the *XMM-Newton* observation was performed  $\sim 3.5$  days after the *RXTE* observation during which the mHz QPO was observed, it means that this QPO lasted less than 3.5 days after the *RXTE* observation. We fitted the *XMM-Newton* PDS also with two zero-centered Lorentzians (similar to what we had done for the *RXTE* data), which provided an acceptable fit ( $\chi^2_{\nu} \sim 1.1$ ). The frequency and rms amplitude of the two Lorentzians are  $0.53 \pm 0.02$  Hz and  $0.030 \pm 0.001$  Hz, and  $18.8 \pm 0.2\%$  and  $26.4 \pm 0.3\%$ , respectively. We also fit the PDS with a broken-power law plus one Lorentzian model resulting in a break frequency of  $0.038 \pm 0.002$  Hz and a frequency of  $0.33 \pm 0.06$  Hz for the Lorentzian. Both fit models gave values which are very similar to what we have obtained from the *RXTE* power spectra. We note that the *XMM-Newton* data covers a different energy range (0.5–10 keV) than the *RXTE* data (2–20 keV), therefore a direct comparison between the results has to be done with care. A detailed timing study (e.g., evolution of the power spectral features, energy dependency) is beyond the scope of this paper.

## 4 DISCUSSION

We report on the spectral and timing behaviour of the VFXT and black hole system Swift J1357.2–0933 as observed with *XMM-Newton* and on the timing behaviour of the source as observed with *RXTE*.

### 4.1 Spectral behaviour

Our high quality *XMM-Newton* spectrum of Swift J1357.2–0933 was acquired one week after the source was discovered. The source was detected at a luminosity of  $L_X \sim 9 \times 10^{34} (D/1.5 \text{ kpc})^2 \text{ erg s}^{-1}$ . The best-fitting model to the spectrum consists of a thermal component (DISKBB) with a temperature of  $kT \sim 0.22$  keV, a hard component (NTHCOMP) with a photon index of  $\Gamma \sim 1.6$  and  $kT_e \sim 8.2$  keV, and one EDGE located at  $\sim 0.73$  keV.

The most probable origin for the thermal component is soft emission from the accretion disc, given that the compact object is a black hole (Corral-Santana et al. 2013). The disc temperature obtained is low compared to the typical 1–2 keV obtained for black hole X-ray transients in their soft states (e.g., McClintock & Remillard 2006). However, similar relatively cool discs are observed in black hole systems in their low-hard state (e.g., Miller et al. 2006a,b; Reis et al. 2010).

The only clear spectral feature detected in the Swift J1357.2–0933 spectrum is an edge at  $\sim 0.73$  keV ( $\sim 17\text{\AA}$ ). This feature is likely due to absorption by interstellar Fe (the L3 edge at  $\sim 0.70$  keV and L2 edge at  $\sim 0.72$  keV have been detected in other LMXBs; e.g., Díaz Trigo et al. 2007; Pinto et al. 2013). But if indeed Swift J1357.2–0933 is an accretion disc corona (ADC) system seen in an edge-on geometry, as suggested by Corral-Santana et al. (2013), we would expect to see more lines in our spectra intrinsic to the source (and not only due to interstellar absorption). Searching in the literature for spectral results of ADC sources, we found that generally they show a variety of absorption and/or emission lines (e.g., Cottam et al. 2001; Kallman et al. 2003; Boirin et al. 2005; Iaria et al. 2013).

Additionally, if Swift J1357.2–0933 were an ADC source, the intrinsic X-ray luminosity of the source would be approximately one to two orders of magnitude higher than the luminosities we observe and therefore the peak of luminosity reached by the source would be  $L_X \sim 10^{36-37} \text{ erg s}^{-1}$ . However, Armas Padilla et al. (2013) found that the spectra of Swift J1357.2–0933 became softer when the source luminosity decreased. Such softening is observed in BH systems at luminosities  $L_X \lesssim 10^{36} \text{ erg s}^{-1}$  (e.g., Plotkin et al. 2013; Corbel et al. 2006). Therefore, the spectral evolution seen for Swift J1357.2–0933 is the expected at the observed X-ray luminosities, suggesting that it is, at least, close to its intrinsic luminosity.

### 4.2 Timing behaviour

The broadband power density spectrum seen with both *XMM-Newton* and *RXTE* resembles, in both the shape as well as the strength of the components, those seen from other black hole X-ray transients at low luminosities. In particular, the power spectrum can be modeled with either two Lorentzians or with a broken power-law model plus a Lorentzian. In the latter case, the break frequency ( $0.038 \pm 0.002$  Hz) and the frequency of the Lorentzian ( $0.33 \pm 0.06$  Hz) obtained using the *XMM-Newton* data fall exactly on the relation found by Wijnands & van der Klis (1999), clearly identifying these components with similar components seen in other black hole systems as well as in neutron star X-ray binaries. However, contrary what is seen in those neutron-star systems (e.g., Sunyaev & Revnivtsev 2000; Linares et al. 2007), we do not see power at frequencies higher than those two components, which is similar to what is seen in other black hole systems. This supports the identification that the accretor in this system is a black hole and not a neutron star (Corral-Santana et al. 2013).

As discussed previously, Corral-Santana et al. (2013) suggested that the source is viewed at very high inclination and an ADC source. However, in our *XMM-Newton* observation, and in the *RXTE* data as well (see also Corral-Santana et al. 2013), we do not see any signs of the 2.8 hr orbit which would be expected for such high inclinations. Corral-Santana et al. (2013) proposed that the absence of any orbital period signature in the X-ray data could be due to the fact that the system has an extreme mass ratio and therefore the very small size of the donor, making an X-ray eclipse very shallow and difficult to detect in Swift J1357.2–0933. It is unclear if this can indeed explain the lack of any orbital signature in the *XMM-Newton* data as well.

The hypothesis for a high inclination was also indicated by the optical dipping behavior of the source (Corral-Santana et al. 2013). No such dipping is visible in the X-ray data obtained with *XMM-Newton*. We also searched the *RXTE* data and found that during the first observation a quasi-periodic oscillation is present in the X-ray data. The QPO is at similar frequencies as the frequency of the optical dips, however, we only see the QPO in the first *RXTE* observation and not in any of the following observations. In particular, no oscillations were seen in the *RXTE* observations closest to the dates of the detection of the optical dips. In addition, the frequency of the optical dips decreased with decreasing X-ray luminosity of the source. Extrapolating the frequency towards the start of the

outburst would give a much higher frequency for the dips or QPO than we observed for the X-ray QPO (see Fig. 1, bottom panel). Therefore, it is not clear whether the mechanism behind the optical dips is similar to that behind the X-ray QPO, or whether we observe two distinct phenomena which happen to produce variation at similar time scales. In the former case, the frequency either first is anti-correlated with X-ray luminosity but later correlated, or we might see different harmonics in the X-rays compared to in the optical. Neither possibility is straightforwardly explained by an inner disc torus moving outwards when the X-ray luminosity decreases (as suggested by Corral-Santana et al. 2013, to explain the optical dips).

Alternatively, the X-ray QPO we observed in Swift J1357.2–0933 could be part of the recently suggested new class of black hole QPOs (Altamirano & Strohmayer 2012): a low frequency QPO with frequencies in the mHz range which is only seen at the start of an outburst. Such a QPO has so far only been seen in one system (namely H1743–322; see Altamirano & Strohmayer 2012) but the properties of the QPO in that system resembles the QPO seen in Swift J1357.2–0933. Both QPOs are at low frequencies (11 mHz versus 6 mHz for H1743–322 and Swift J1357.2–0933 respectively) and only seen at the start of an outburst<sup>3</sup> (although we note that the upper limits on the QPO strength after the first observation of Swift J1357.2–0933 are not very constraining so this QPO might have been present during some later observations as well). We suggest that the QPO seen in Swift J1357.2–0933 is indeed similar to the QPO seen in H1743–322, making Swift J1357.2–0933 the second black hole system in which this QPO is seen.

Altamirano & Strohmayer (2012) compared this "mHz QPO" with other QPOs seen in black hole and neutron star X-ray binaries and they concluded that it best resembled the so-called "1 Hz QPO" seen in dipping (and thus at relatively high inclination) neutron star systems (Jonker et al. 1999, 2000; Homan et al. 1999; Bhattacharyya et al. 2006; Homan 2012), although at significantly lower (a factor of 10–100) frequencies. This 1 Hz QPO could be due to a structure in the inner disc which quasi-periodically obscures the inner region (Jonker et al. 1999), although recently it was proposed that these QPOs might be due to relativistic Lense-Thirring precession of the inner accretion disc (Homan 2012). Altamirano & Strohmayer (2012) suggested that the difference in frequency of the mHz QPO and the 1 Hz QPO might be explained if the frequency of the QPO scales with the mass, or that it might depend on the orbital period of the system (the orbital period of H1743–322 might be significantly longer than the orbital period of the dipping neutron star systems which exhibited this QPO). However, if the QPO in Swift J1357.2–0933 is due to the same mechanism as the QPO in H1743–322 and if they are related to the 1 Hz QPOs, then the orbital period is not relevant because the orbital period of Swift J1357.2–0933 is only 2.8 h, leaving only the mass of the accretor as a potential determinant for the exact observed QPO frequency.

<sup>3</sup> We note that in H1743–322, when it was present, the QPO was seen only at the start of an outburst, but not every outburst of the source shows the QPO even if ample data were available; Altamirano & Strohmayer (2012)

We note that it cannot be conclusively stated that the X-ray QPO we see in Swift J1357.2–0933 is indeed related to the 1 Hz QPO in the dipping neutron star systems, however, it is intriguing that a high inclination was also inferred (Corral-Santana et al. 2013) for Swift J1357.2–0933, similar to the dipping neutron star systems. This then would support the hypothesis that the X-ray QPO in Swift J1357.2–0933 might still be related to the optical dips seen from the systems, although it is currently not clear how exactly all observed phenomena can be explained consistently.

## 5 FINAL REMARKS

The X-ray spectral and timing properties we have observed for Swift J1357.2–0933 in combination with the optical dips seen in outburst by Corral-Santana et al. (2013), presents us with a complex range of phenomena which needs to be explained. From the X-ray and optical timing behavior (in combination with the broad width of the observed  $H_\alpha$  line) it was suggested that the source is at a relatively high inclination. Corral-Santana et al. (2013) suggested even such a high inclination that we see the source edge on and the X-rays might then only be due to scattered light (originating from the inner region near the black hole) in an ADC. This might explain the optical dips, the low observed X-ray luminosities (intrinsically the luminosity would be much higher) and the broad  $H_\alpha$  profile (Corral-Santana et al. 2013). However, the lack of orbital modulation in the X-rays (neither eclipses nor the characteristic X-ray dips were seen) and the lack of strong emission or absorption lines in the X-ray spectrum obtained with *XMM-Newton* cast doubt on this edge-on hypothesis. In addition, a lower inclination might also allow for an alternative (at least partly) explanation (then the one suggested by Shahbaz et al. 2013) why the orbital modulation in the companion star flux could not be detected (lower inclination gives rise to lower amplitude of this modulation) in quiescence and why in quiescence the  $H_\alpha$  line was not double peaked (lower inclination gives rise to less separated lines). Furthermore, we see clearly a soft thermal component at low energies in the *XMM-Newton* spectrum which probably originates from the inner edge of the disc, also strongly indicating that we can observe directly the inner part of the system. Therefore, we suggest that the system is still at relatively high inclination so that the obscuring region which causes the optical dips and the X-ray QPO still intersect periodically our line of sight to the inner part of the system, but that the inclination is not high enough to permanently obscure our view from the inner part. This would mean that the luminosity we observe from Swift J1357.2–0933 is its intrinsic luminosity and therefore the source is indeed a VFXT. Why the source has such a low intrinsic luminosity and how exactly the optical dips and X-ray QPO are produced remains to be determined.

## ACKNOWLEDGMENTS

We acknowledge the *XMM-Newton* team for make this observation possible. RW and MAP are supported by an European Research Council starting grant awarded to RW. ND

is supported by NASA through Hubble Postdoctoral Fellowship grant number HST-HF-51287.01-A from the Space Telescope Science Institute (STScI).

## REFERENCES

- Armas Padilla M., Degenaar N., Russell D. M., Wijnands R., 2013, *MNRAS*, 428, 3083
- Arnaud K. A., 1996, in Jacoby G. H., Barnes J., eds, *Astronomical Data Analysis Software and Systems V* Vol. 101 of *Astronomical Society of the Pacific Conference Series*, XSPEC: The First Ten Years. p. 17
- Altamirano, D., & Strohmayer, T. 2012, *ApJL*, 754, L23
- Altamirano, D., van der Klis, M., Méndez, M., et al. 2008, *ApJ*, 685, 436
- Barthelmy S. D., Barbier L. M., Cummings J. R., Fenimore E. E., Gehrels N., Hullinger D., Krimm H. A., Markwardt C. B., Palmer D. M., Parsons A., Sato G., Suzuki M., Takahashi T., Tashiro M., Tueller J., 2005, *Space Sci. Rev.*, 120, 143
- Belloni, T., Psaltis, D., & van der Klis, M. 2002, *ApJ*, 572, 392
- Belloni, T., & Hasinger, G. 1990, *A&A*, 227, L33
- Bhattacharyya, S., Strohmayer, T. E., Markwardt, C. B., & Swank, J. H. 2006, *ApJL*, 639, L31
- Boirin, L., Méndez, M., Díaz Trigo, M., Parmar, A. N., & Kaastra, J. S. 2005, *A&A*, 436, 195
- Casares, J., Torres, M. A. P., Negueruela, I., et al. 2011, *The Astronomer's Telegram*, 3206, 1
- Chelovekov I. V., Grebenev S. A., 2007, *Astron. Lett.*, 33, 807
- Corbel, S., Tomsick, J. A., & Kaaret, P. 2006, *ApJ*, 636, 971
- Cornelisse R., Verbunt F., in't Zand J. J. M., Kuulkers E., Heise J., Remillard R. A., Cocchi M., Natalucci L., Bazzano A., Ubertini P., 2002, *A&A*, 392, 885
- Corral-Santana J. M., Casares J., Muñoz-Darias T., Rodríguez-Gil P., Shahbaz T., Torres M. A. P., Zurita C., Tyndall A. A., 2013, *Science*, 339, 1048
- Cottam, J., Sako, M., Kahn, S. M., Paerels, F., & Liedahl, D. A. 2001, *ApJL*, 557, L101
- Degenaar N., Wijnands R., 2009, *A&A*, 495, 547
- Degenaar N., Wijnands R., 2010, *A&A*, 524, 69
- Del Santo M., Sidoli L., Mereghetti S., Bazzano A., Tarana A., Ubertini P., 2007, *A&A*, 468, L17
- den Herder J. W., Brinkman A. C., Kahn S. M., Branduardi-Raymont G., Thomsen K., Aarts H., 2001, *A&A*, 365, L7
- Díaz Trigo M., Parmar A. N., Miller J., Kuulkers E., Caballero-García M. D., 2007, *A&A*, 462, 657
- Díaz Trigo M., Sidoli L., Boirin L., Parmar A. N., 2012, *A&A*, 543, A50
- Dunn R. J. H., Fender R. P., Körding E. G., Belloni T., Cabanac C., 2010, *MNRAS*, 403, 61
- Gierliński M., Zdziarski A. A., Poutanen J., Coppi P. S., Ebisawa K., Johnson W. N., 1999, *MNRAS*, 309, 496
- Hiemstra B., Méndez M., Done C., Díaz Trigo M., Altamirano D., Casella P., 2011, *MNRAS*, 411, 137
- Homan, J. 2012, *ApJL*, 760, L30
- Homan, J., Jonker, P. G., Wijnands, R., van der Klis, M., & van Paradijs, J. 1999, *ApJL*, 516, L91
- Iaria, R., Di Salvo, T., D'Ai, A., et al. 2013, *A&A*, 549, A33
- Jansen F., Lumb D., Altieri B., Clavel J., Ehle M., Erd C., Gabriel C., Guainazzi M., Gondoin P., Much R., Munoz R., Santos M., Scharrel N., Texier D., Vacanti G., 2001, *A&A*, 365, L1
- Jonker, P. G., van der Klis, M., & Wijnands, R. 1999, *ApJL*, 511, L41
- Jonker, P. G., van der Klis, M., Homan, J., et al. 2000, *ApJ*, 531, 453
- Kallman, T. R., Angelini, L., Boroson, B., & Cottam, J. 2003, *ApJ*, 583, 861
- King, A. R., & Wijnands, R. 2006, *MNRAS*, 366, L31
- Kirsch M. G. F., Altieri B., Chen B., Haberl F., Metcalfe L., Pollock A. M., Read A. M., Saxton R. D., Sembay S., Smith M. J., 2004, in Hasinger G., Turner M. J. L., eds, *Society of Photo-Optical Instrumentation Engineers (SPIE) Conference Series* Vol. 5488 of *Society of Photo-Optical Instrumentation Engineers (SPIE) Conference Series*, XMM-Newton (cross)-calibration. pp 103–114
- Klein Wolt, M. 2004, Ph.D. Thesis,
- van der Klis, M. 1995, *The Lives of the Neutron Stars*, 301
- Krimm H. A., Barthelmy S. D., Baumgartner W., Cummings J., Fenimore E., Gehrels N., Markwardt C. B., Palmer D., Sakamoto T., Skinner G., Stamatikos M., Tueller J., Ukwatta T., 2011a, *The Astronomer's Telegram*, 3138, 1
- Krimm, H. A., Kennea, J. A., & Holland, S. T. 2011b, *The Astronomer's Telegram*, 3142, 1
- Linares, M., van der Klis, M., & Wijnands, R. 2007, *ApJ*, 660, 595
- Lomb, N. R. 1976, *Ap&SS*, 39, 447
- Maeda Y., Koyama K., Sakano M., Takeshima T., Yamauchi S., 1996, *PASJ*, 48, 417
- Makishima K., Maejima Y., Mitsuda K., Bradt H. V., Remillard R. A., Tuohy I. R., Hoshi R., Nakagawa M., 1986, *ApJ*, 308, 635
- McClintock, J. E., Haswell, C. A., Garcia, M. R., et al. 2001, *ApJ*, 555, 477
- McClintock, J. E., & Remillard, R. A. 2006, *Compact stellar X-ray sources*, 157
- Milisavljevic, D., Fesen, R. A., Parrent, J. T., & Thorstensen, J. R. 2011, *The Astronomer's Telegram*, 3146, 1
- Miller, J. M., Homan, J., Steeghs, D., et al. 2006a, *ApJ*, 653, 525
- Miller, J. M., Homan, J., & Miniutti, G. 2006b, *ApJL*, 652, L113
- Miyamoto, S., Kimura, K., Kitamoto, S., Dotani, T., & Ebisawa, K. 1991, *ApJ*, 383, 784
- Pinto C., Kaastra J. S., Costantini E., de Vries C., 2013, *A&A*, 551, A25
- Plotkin, R. M., Gallo, E., & Jonker, P. G. 2013, *arXiv:1306.1570*
- Rau A., Greiner J., Filgas R., 2011, *The Astronomer's Telegram*, 3140, 1
- Reis, R. C., Fabian, A. C., & Miller, J. M. 2010, *MNRAS*, 402, 836
- Scargle, J. D. 1982, *ApJ*, 263, 835
- Shahbaz, T., Russell, D. M., Zurita, C., et al. 2013, *arXiv:1307.0659*
- Strüder L., Briel U., Dennerl K., Hartmann R., Kendziorra



- E., Meidinger N., Pfeffermann E., Reppin C., et al. 2001, A&A, 365, L18
- Sunyaev, R., & Revnivtsev, M. 2000, A&A, 358, 617
- Torres, M. A. P., Steeghs, D., Jonker, P. G., & Rauch, M. 2011, The Astronomer's Telegram, 3143, 1
- Turner M. J. L., Abbey A., Arnaud M., Balasini M., Barbera M., Belsole E., Bennie P. J., Bernard J. P., et al. 2001, A&A, 365, L27
- Verner D. A., Ferland G. J., Korista K. T., Yakovlev D. G., 1996, ApJ, 465, 487
- Wijnands, R., & van der Klis, M. 1999, ApJ, 514, 939
- Wijnands R., Homan J., Miller J. M., Lewin W. H. G., 2004, ApJL, 606, L61
- Wijnands R., in't Zand J. J. M., Rupen M., Maccarone T., Homan J., Cornelisse R., Fender R., Grindlay J., van der Klis M., Kuulkers E., Markwardt C. B., Miller-Jones J. C. A., Wang Q. D., 2006, A&A, 449, 1117
- Wijnands R., Rol E., Cackett E., Starling R. L. C., Remillard R. A., 2009, MNRAS, 393, 126
- Wilms J., Allen A., McCray R., 2000, ApJ, 542, 914
- Zhang, W., Giles, A. B., Jahoda, K., et al. 1993, SPIE, 2006, 324
- Zhang, W., Jahoda, K., Swank, J. H., Morgan, E. H., & Giles, A. B. 1995, ApJ, 449, 930
- Zdziarski A. A., Johnson W. N., Magdziarz P., 1996, MNRAS, 283, 193
- Życki P. T., Done C., Smith D. A., 1999, MNRAS, 309, 561